GDCh

Research Articles

Angewandte
Chemie
International Edition
www.angewandte.org

Aqeous Zn Batteries Hot Paper

pH-Triggered Molecular Switch Toward Texture-Regulated Zn Anode

Shao-Jian Zhang[+], Junnan Hao[+], Yilong Zhu[+], Huan Li, Zhan Lin,* and Shi-Zhang Qiao*

Abstract: Zn electrodes in aqueous media exhibit an unstable Zn/electrolyte interface due to severe parasitic reactions and dendrite formation. Here, a dynamic Zn interface modulation based on the molecular switch strategy is reported by hiring γ-butyrolactone (GBL) in $ZnCl_2/H_2O$ electrolyte. During Zn plating, the increased interfacial alkalinity triggers molecular switch from GBL to γ-hydroxybutyrate (GHB). GHB strongly anchors on Zn surface via triple Zn–O bonding, leading to suppressive hydrogen evolution and texture-regulated Zn morphology. Upon Zn stripping, the fluctuant pH turns the molecular switch reaction off through the cyclization of GHB to GBL. This dynamic molecular switch strategy enables high Zn reversibility with Coulombic efficiency of 99.8% and Zn‖iodine batteries with high-cyclability under high Zn depth of discharge (50%). This study demonstrates the importance of dynamic modulation for Zn electrode and realizes the reversible molecular switch strategy to enhance its reversibility.

Introduction

Aqueous Zn-ion batteries (AZIBs) are overwhelming technologies for large-scale energy storage owing to their inherent safety and low price.[1] However, the instable Zn/electrolyte interface leads to poor reversibility of Zn anodes, as reflected by severe dendrite formation and water-related parasitic reactions.[2] The parasitic hydrogen evolution

[*] S.-J. Zhang,[+] Dr. J. Hao,[+] Y. Zhu,[+] Dr. H. Li, Prof. S.-Z. Qiao
School of Chemical Engineering & Advanced Materials, The University of Adelaide
Adelaide, SA-5005 (Australia)
E-mail: s.qiao@adelaide.edu.au

Prof. Z. Lin
Guangdong Provincial Key Laboratory of Plant Resources Biorefinery, School of Chemical Engineering and Light Industry, Guangdong University of Technology
Guangzhou 510006 (China)
E-mail: zhanlin@gdut.edu.cn

[+] These authors contributed equally to this work.

reaction (HER) releases flammable and explosive hydrogen (H_2) gas, which significantly compromises the high-safety nature of AZIBs. HER has been demonstrated to accelerate the formation of Zn^{2+}-insulating layered double hydroxide (LDH) precipitates, which disturbs the ion flux and further exacerbates dendrite growth.[3] Tremendous efforts including solvation optimization,[4] additive strategies,[5] surface modifications,[6] etc., have been proposed to enhance the Zn reversibility. However, the repeated Zn plating/stripping would renew the Zn/electrolyte interface constantly, which raises challenges to efficiently modulate Zn/electrolyte interface dynamically.

Molecular switches are defined as molecules that can reversibly change their conformations and relative properties under external influence, such as pH, irradiation etc,[7] which have been widely applied as ion sensor, drug delivery, catalysts, etc.[8] In AZIBs, the repeated Zn plating/stripping processes accompanied by HER results in the periodical pH evolution at the Zn surface.[9] The periodical fluctuation of H^+/OH^- may be feasible to trigger the pH-dependent molecular switch reaction to modulate Zn/electrolyte interface dynamically. Lactone is a kind of cyclic compounds which contain lactone bonding. Alkyl-oxygen linkage in lactone bonding can be cleaved and re-constructed reversibly under the given chemical environment. Among the variety of lactones, γ-butyrolactone (GBL) has a high donor number (18.0) and high miscibility with H_2O in any ratios,[10] endowing GBL a promising co-solvent in AZIBs. Previous demonstrations revealed that molecules with rich polar functional groups are likely to be efficient in interface modulation.[5a, 11] Thus, the cyclic GBL is predicted to have less contribution to interface modulation, despite it can significantly function in manipulating the bulk solvation configuration. GBL is stable in the acid environment, while it will open the ring structure by forming γ-hydroxybutyrate (GHB) in alkaline environment through the hydrolysis reaction. Compared to the cyclic GBL, GHB molecule has two polar endings (–OH and $–COO^-$), enabling its strong ability to modify the Zn surface. When the ambient environment returns to acidity, GHB can be re-cyclized to GBL via intramolecular esterification mechanism.[12] This characteristic conversion well agrees on the periodic pH evolution of Zn surface during cycling, implying its ability of dynamic modulation on the Zn/electrolyte interface.

Here, the molecular switch strategy is reported to create a dynamic Zn/electrolyte interface relying on the periodical pH evolution of Zn anodes. In bulk electrolyte, GBL anticipates the Zn^{2+} solvation configuration, which declines the activity of coordinated H_2O in the solvation sheath and

benefits to Zn de-solvation (Figure 1a). At the Zn/electrolyte interface, the reversible transformation between GBL and GHB depending on the dynamic interfacial pH evolution is validated during Zn plating/stripping. During Zn plating, the alkaline Zn/electrolyte interface triggers the lactone hydrolysis of GBL to generate GHB (Figure 1b). The generated GHB presents strong adsorption with Zn (002) facet by the triple Zn–O bonding (Figure 1c), resulting in a dense, texture-regulated, and dendrite-free Zn morphology. This dynamic interface modulation induces a leading on-set potential for Zn plating, while postpones the on-set potential for HER, as monitored by the real-time differential electrochemical mass spectrometry (DEMS). During Zn stripping, the acid electrolyte environment renders the intermolecular esterification reaction of GHB to re-generate GBL (Figure 1d), which further returns to bulk electrolyte and involves the Zn^{2+} solvation configuration again. Based on this molecular switch mechanism, the dynamic modulation of Zn/electrolyte interface is achieved. Comprehensive evidence validates the enhanced reversibility of Zn anodes, as strongly highlighted by its high Coulombic efficiency (CE) of 99.8 % for 500 cycles at $2\,mA\,cm^{-2}$ and 99.8 % for 800 cycles at $30\,mA\,cm^{-2}$. As a proof-to-concept, $Zn||I_2$ batteries under high Zn depth of discharge (DOD,50 %) realizes a long-term cyclability of 2000 cycles with a capacity retention of 81.9 %. This molecular switch mechanism is also proved to take effect under an extremely low temperature ($-30\,°C$) with compact Zn morphology, admirable Zn reversibility with an average Zn CE of 99.9 %, and excellent full cell durability (10 000 cycles for $Zn||$ polyaniline (PANI) battery).
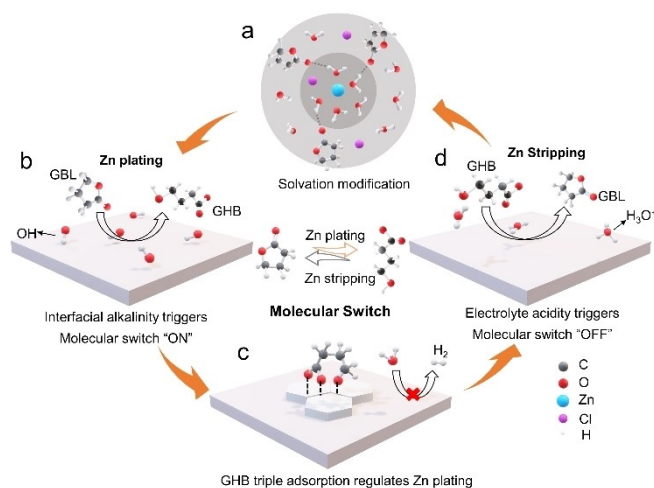

Figure 1. Scheme of the functions of GBL-GHB molecular switch. a) Modification of solvation configuration by GBL. b) Molecular switch "on" during Zn plating. c) Impacts of molecular switch reaction on modulating Zn/electrolyte interface. d) Molecular switch "off" during Zn stripping.

Results and Discussion

Functions of GBL in electrolyte

GBL has almost no capacity to dissolute $ZnCl_2$, while it presents high miscibility with $ZnCl_2/H_2O$ electrolyte in any ratios (Figure S1). GBL is a flammable organic solvent, however, the GBL-containing $ZnCl_2/H_2O$ electrolytes can maintain nonflammable when the volum ratio of GBL is less than 90 Vol % (Figure S2), ensuring the high-safety nature of AZIBs. Raman spectra were collected to identify the functions of GBL in $ZnCl_2/H_2O$ electrolytes. As depicted in Figure S3, GBL has a sharp Raman peak situated at $1764\,cm^{-1}$, which is associated with the C=O stretching vibration of GBL. When GBL is dissolved into $ZnCl_2/H_2O$ electrolyte, a new peak located at $1746\,cm^{-1}$ is detected, confirming the hydrogen bond (H-bond) formation between H_2O–GBL.[13] Around 80 % GBL molecules participate in the H_2O-GBL H-bond formation when the volume ratio of GBL is $\leq 40\,vol\,\%$. When the ratio of GBL increases, the intensified peak of free GBL can be observed in $ZnCl_2/H_2O$ electrolytes, implying the optimal GBL ratio in electrolyte of 40 vol %. The addition of GBL in $ZnCl_2/H_2O$ electrolyte would decrease the ionic conductivity. Nevertheless, the GBL-containing electrolyte still maintains a high ionic conductivity of $36.1\,mS\,cm^{-1}$ when the GBL content is 40 Vol % (Figure S4).

The impact of GBL in modifying Zn^{2+} solvation configuration was conducted by molecular simulation (MD) (Figure S5). In the pure $ZnCl_2/H_2O$ electrolyte, around 5.85 H_2O molecules are anticipated to coordinate with Zn^{2+} in the first solvation sheath. By contrast, in $ZnCl_2/H_2O$-40GBL, the coordination number of H_2O molecules declines to 5.46 per Zn^{2+}, while only 0.07 GBL per Zn^{2+} in the first solvation sheath. This solvation configuration modulation of GBL can be convinced by Raman spectra with declination of H_2O-containing solvation configuration, which benefits to the Zn de-sovlation (Figure S6). Moreover, the H-bond formation between water and GBL reduces water activity, contributing to the suppression of HER.[14]

Molecular switch mechanism

GBL shows a huge potential to be a reversible molecular switch for modifying Zn/electrolyte interface relying on the pH evolution. As shown in Figure S7, a strong peak in Fourier-transform infrared spectroscopy (FTIR) spectra located at $1756\,cm^{-1}$ can be observed in the GBL aqueous solution, which is associated with C=O stretching vibration mode of GBL molecules.[15] When the pH value increases to 10, a new peak located at $1556\,cm^{-1}$ can be detected. This peak can be identified as the C=O vibration in dissociative carboxyl groups (–COO^-) of GHB, which is the ring-open product of GBL.[16] As the pH value returns to 5, the vibration of C=O in carboxyl groups disappears, indicating the re-cyclization of GHB by forming GBL. Compared to GBL, GHB with two polar functional endings (–OH and –COO^-) are more likely to occupy the Zn surface, which is

Angew. Chem. Int. Ed. **2023**, e202301570 (2 of 8)

© 2023 The Authors. Angewandte Chemie International Edition published by Wiley-VCH GmbH

predicted to have a stronger ability to modulate the Zn/electrolyte interface. This reversible molecular conversion dependant on the pH fluctuation matches well with the periodic pH variation on the Zn surface during its plating/stripping process, which validates its possibility as a molecular switch to dynamically regulate the Zn/electrolyte interface.

To verify the feasibility of the molecular switch, in-situ FTIR was conducted during Zn plating/stripping. As displayed in Figure 2a, the GBL-containing electrolyte is used as background to collect FTIR spectra, thus there are not any signals at open circuit potential. In FTIR spectra, the downward peaks stand for the production formation, while the upward peaks mean the reactant consumption. A pair of gradually intensified upward and downward peaks ($1760 \ cm^{-1}$ and $1521 \ cm^{-1}$) can be observed during Zn plating, illustrating the generation of GHB and the consumption of GBL. This validates the "on" state of GBL-to-GHB molecular switch during Zn plating. While a synchronous declination of the C=O vibration of GBL and the consumption of GHB can be found in Zn stripping, meaning an opposite "off" state of GHB-to-GBL molecular switch. The molecular switch process between GBL and GHB is also summarized in Figure 2b, which matches well with the Zn plating and stripping. To give an insight into the pathways of molecular switch reaction, DFT calculation was conducted to simulate the pH-triggered conformation changes between GBL and GHB. Three types of relevant energies of all intermediates, including zero-point energy, entropy, and Gibbs free energy, are listed in Table S1 and

S2. As shown in Figure 2c, the final state of GHB salt presents a lower Gibbs free energy compared to the initial state (GBL+OH$^-$) with an energy gap of 1.255 eV, verifying the thermodynamic feasibility from GBL to GHB in the alkaline environment. Meanwhile, the Gibbs free energy of the transition state falls in the energy range between initial and final states, indicating the spontaneity of the GBL-to-GHB reaction. For the reversed process, the GHB-to-GBL transformation is also feasible by overcoming a small energy barrier (+0.102 eV) (Figure S8).

The specific "on" and "off" mechanisms of molecular switch reactions are given. The "on" state of GBL-to-GHB molecular switch reaction obeys the base-catalysis mechanism.[12a] Although GBL is stable in the acid media, it can be hydrolyzed in alkaline environment by cleaving the alkyl-oxygen bonding. During Zn plating, the surplus hydroxyl ion at the Zn/electrolyte interface attacks the carbonyl carbon of GBL by yielding a cyclic intermediate. And this cyclic intermediate is unstable and then decomposes to form GHB (Figure 2d). While during Zn stripping, GHB returns to bulk electrolyte with the stripped Zn^{2+}. And the acid environment of electrolyte triggers the intermolecular esterification reaction of GHB. As depicted in Figure 2e, the carbonyl group of GHB is firstly protonated, and then the terminal hydroxyl group attacks the carbonyl carbon of GHB to proceed with a cyclization reaction by re-generating GBL. This reversible molecular switch reaction depends on the pH evolution of the Zn surface, endowing GBL-GHB molecular switch with the ability to dynamically modulate the Zn/electrolyte interface.
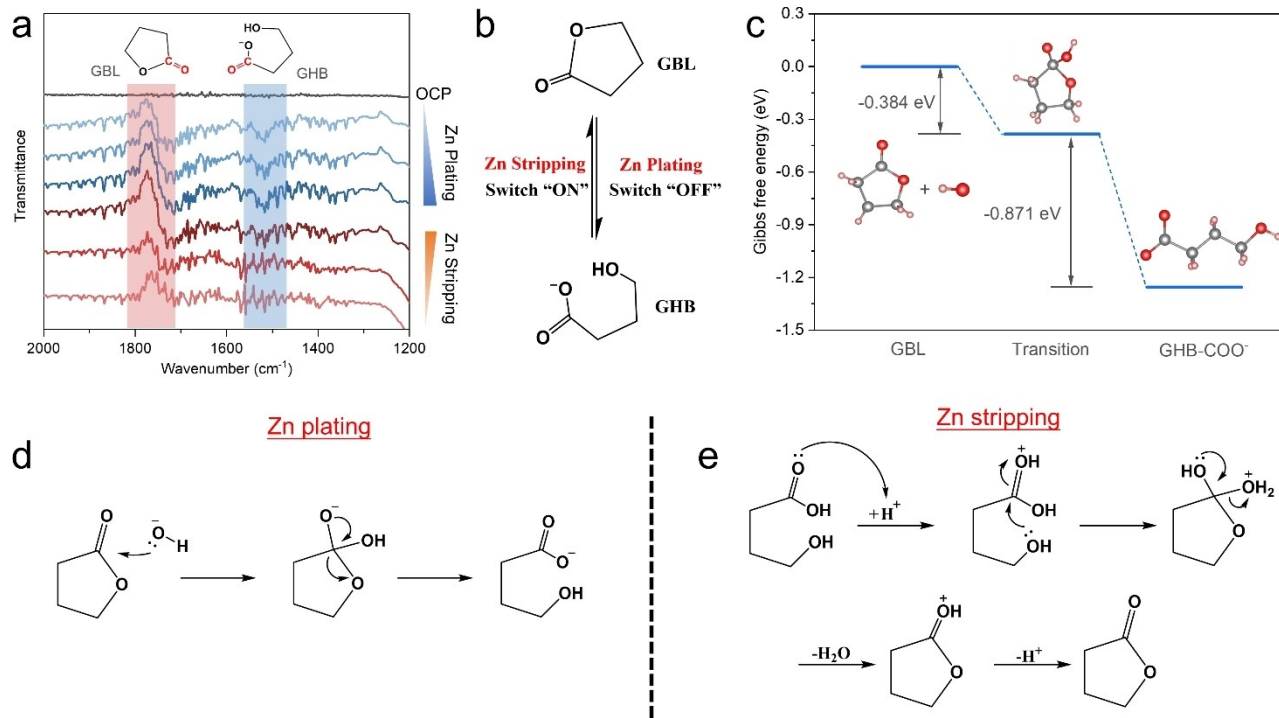

Figure 2. Molecular switch behaviour at the Zn/electrolyte interface. a) In situ FTIR of the Zn/electrolyte interface upon Zn plating/stripping. b) Corresponding conformation changes between GBL and GHB. c) The reaction pathway of the molecular switch on the reaction from GBL to GHB. The reaction mechanism of conformation changes between GBL and GHB during d) Zn plating and e) Zn stripping.

Zn/electrolyte interface modulation by molecular switch

DFT calculation was carried out to reveal the impact of the molecular switch mechanism on tuning the Zn/electrolyte interface (Figure 3a). GBL presents a weak interaction with Zn (002) facet (-0.50 eV), which is only slightly stronger than H_2O (-0.25 eV), implying insufficient interface modulation ability. The molecular switch "on" reaction can generate GHB during Zn plating to stabilize the Zn/electrolyte interface. This is because the polar $-OH$ (-0.57 eV) and $-COO*$ (-2.87 eV) terminals of GHB have stronger interaction with Zn (002) facet compared to free H_2O and GBL. Optimal structure reveals that GHB can strongly anchor on the Zn (002) facet via triple Zn–O bonding with the lowest binding energy of -2.99 eV, demonstrating GHB can adsorb on the Zn surface more preferentially. The charge density distribution between Zn slab and GHB indicates that GHB induces extra charge at the Zn surface, manifesting its strong electrostatic adsorption (Figure 3b). Preferential adsorption of GHB at the Zn surface was proved to prevent the H_2O-relative parasitic reactions.[5a, 11]

The low redox potential of Zn/Zn^{2+} couple inevitably causes HER in aqueous media during the Zn plating.[17] To evaluate HER in AZIBs, linear sweep voltammetry (LSV) is the most prevalent method.[11] However, both Zn plating and HER contribute to the current response in LSV curves at a similar potential range, leading to the failure identification for the on-set potential of Zn plating and HER, respectively. Several reports adopted Na_2SO_4 to replace $ZnSO_4$ to avoid the confusion of HER and Zn plating.[18] Nevertheless, it cannot veritably reflect HER during Zn plating owing to the absence of Zn^{2+}-related electrochemical behavior. DEMS can real-time monitor the gas evolution during electrochemical process, which can precisely distinguish the on-set potential of Zn plating and HER. As shown in Figure 3c, the gold (Au) is coated on a polytetrafluoroethylene (PTFE) film through a magnetron sputtering, which serves as the working electrode. This porous Au-PTFE electrode allows the gas to pass through but blocks the liquid electrolyte. The concomitant H_2 during Zn plating can be real-time collected by the vacuum chamber below the Au-PTFE working electrode, and further monitored by mass spectrometer. Figure 3d compares LSV curves together with mass response of H_2 evolution. In $ZnCl_2/H_2O$-40GBL electrolyte, the current response occurs at -0.96 V vs. Ag/AgCl, which is ahead of that in $ZnCl_2/H_2O$ electrolyte (-1.00 V vs. Ag/AgCl). At this stage, there is no mass response indicating that the current response can only be attributed to Zn plating without H_2 generation. It is worth noting that the HER occurs in $ZnCl_2/H_2O$-40GBL electrolyte below -1.10 V vs. Ag/AgCl, more negative than that in $ZnCl_2/H_2O$ electrolyte (-1.05 V vs. Ag/AgCl). When the reductive potential reaches -1.2 V, much stronger H_2 signal can be detected in $ZnCl_2/H_2O$ electrolyte, revealing the serious side reactions. The $ZnCl_2/H_2O$-40GBL electrolyte enables an ahead on-set potential for Zn plating but a later on-set potential for HER, which indicates the facilitated Zn plating and suppressed HER. This result aslo is evidenced by in-situ gas chromatography (GC) with suppressive HER during continuous Zn plating in $ZnCl_2/H_2O$-40GBL electrolyte (Figure S9). Besides, the GBL also extends the oxidation limitation of electrolytes from 1.6 V to 1.8 V vs. Zn/Zn^{2+}, further demonstrating the GBL can broaden the potential window of electrolytes (Figure S10).

Morphology evolution

The Zn plating morphology in two electrolytes was investigated by scanning electron microscope (SEM). In $ZnCl_2/H_2O$ electrolyte, the plated Zn presents a porous and dendrite morphology (Figure 4a and S7). In sharp contrast, a uniform and dendrite-free Zn plating surface is obtained in the $ZnCl_2/H_2O$-40GBL electrolyte under a wide range of current densities from 1 mA cm^{-2} to 50 mA cm^{-2} (Figure 4b and S11). The high-resolution SEM image reveals a well-defined and texture-regulated Zn plating morphology in the electrolyte of $ZnCl_2/H_2O$-40GBL (inset in Figure 4b). The cross-section SEM morphology provides more intuitive evidence for Zn plating modulation by molecular switch additive. In $ZnCl_2/H_2O$ electrolyte, massive Zn protrusions grow along the vertical direction of the Cu substrate, verifying the uneven Zn plating and dendrite formation (Figure 4c). Remarkably, a compact and dense Zn deposition layer can be observed, emphasizing the uniform Zn plating achieved by GBL-induced dynamic interfacial modulation (Figure 4d). Uniform Zn plating behavior in $ZnCl_2/H_2O$-40GBL without protrusion/dendrite formation was also observed by in situ optical microscopy during the whole Zn plating process (Figure S12).
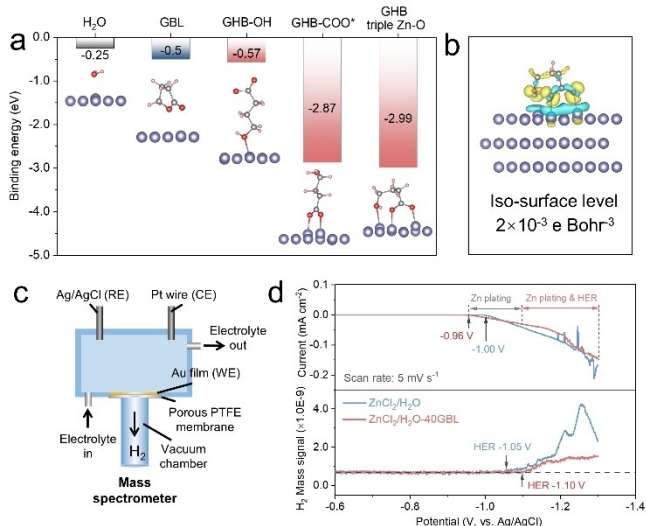

Figure 3. Zn interface modulation by molecular switch. a) Adsorption energy comparison of H_2O and various molecules on the Zn (002) facet. b) Charge density difference of the GHB triple adsorption on the Zn slab along the Z axis. c) The schematic diagram of an electrochemical cell for DEMS. d) DEMS characterizations to identify HER during Zn plating.
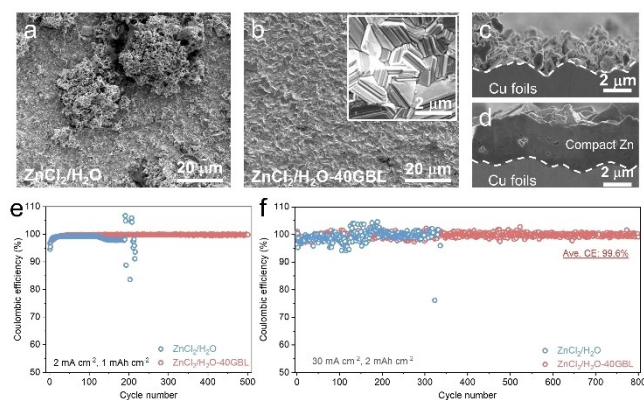
Figure 4. Zn plating/stripping reversibility. Zn plating morphology in a), c) $ZnCl_2/H_2O$ and b), d) $ZnCl_2/H_2O$-40GBL at 2 mA cm^{-2}, 2 mAh cm^{-2}. e) Zn CEs examination in two electrolytes at (e) 2 mA cm^{-2}, 1 mAh cm^{-2} and f) 30 mA cm^{-2}, 2 mAh cm^{-2}.

Electrochemical characterization of Zn anodes

The CE of the Zn plating/stripping in Cu||Zn cells was studied in the electrolyte of $ZnCl_2$ with/without GBL, because parasitic reactions and battery failure of Zn anodes can be reflected by the CE evolution. The Cu||Zn cell with $ZnCl_2/H_2O$ electrolyte presents inferior Zn plating/stripping reversibility with an initial CE of 94.1% and an average CE of 97.1%, whereas it suffers from battery failure only after 40 cycles at 0.5 mA cm^{-2} and 0.5 mAh cm^{-2} (Figure S13). Such a low CE and short battery life verify the serious parasitic reactions and uncontrollable Zn dendrite growth in $ZnCl_2/H_2O$ electrolyte. In comparison, the Zn CE of the Cu||Zn cell reaches a stable value of 99.6% after activation in $ZnCl_2/H_2O$-40GBL electrolyte. $ZnCl_2/H_2O$-40GBL electrolyte also enables high Zn CE of 99.8% for 500 cycles under a current density of 2 mA cm^{-2} (Figure 4e), whilst battery failure occurs after 190 cycles in $ZnCl_2/H_2O$ electrolyte. Charge-discharge curves reveal that the addition of GBL slightly affects the battery polarization but effectively extends the cycling life with negligible polarization increase after 500 cycles (Figure S14). When the current density increases to 30 mA cm^{-2}, the $ZnCl_2/H_2O$-40GBL electrolyte still enables the high Zn reversibility with an average CE of 99.6% for 800 cycles (Figure 4f). An ignorable over-potential increment after cycles further demonstrates the stable Zn/electrolyte interface even under high current density (Figure S15). Whereas, in $ZnCl_2/H_2O$ electrolyte, the stable Zn plating/stripping can withstand only 320 cycles and then suffers from short circuits in the following cycles.

The stable Zn/electrolyte interface modulated by the molecular switch strategy was also validated by the Zn||Zn symmetric cells. The $ZnCl_2/H_2O$-40GBL electrolyte enables Zn||Zn symmetric cell to undergo a decent voltage response without short circuits under step-wisely increased current densities from 1 to 30 mA cm^{-2} (Figure S16). As a comparison, the cell using $ZnCl_2/H_2O$ electrolyte suffers from a short circuit when the current density reaches 20 mA cm^{-2}. The calculated potential polarization also

validates that the $ZnCl_2/H_2O$-40GBL endows a stable Zn/electrolyte interface with smaller polarization compared to the cell using $ZnCl_2/H_2O$ electrolyte. Moreover, it also proceeds a steady Zn plating/stripping for 1500 cycles (600 h) with negligible voltage fluctuation (Figure S17). As for $ZnCl_2/H_2O$ electrolyte, the regular Zn plating/stripping is broken after only 285 cycles due to the short circuit. As demonstrated by SEM, the Zn anode cycled in $ZnCl_2/H_2O$ electrolyte presents a porous and dendritic surface. And the mossy cycled Zn layer and serious Zn corrosion holes can also be observed from the cross section of SEM image (Figure S18). In contrast, the uniform and texture-regulated morphology of the Zn electrode can be found after cycling in $ZnCl_2/H_2O$-40GBL electrolyte. X-ray diffraction (XRD) patterns of cycled Zn electrodes in $ZnCl_2/H_2O$-40GBL electrolyte show that the intensity of Zn (002) peak is enhanced, which further verifies the function of GBL-GHB molecular switch strategy on regulating the orientation of Zn crystals with more Zn (002) exposure (Figure S19). This Zn (002) was also reported as its steady facet on suppression of both dendrite and HER in aqueous media.[19] Besides, both XRD patterns and element analysis confirmed the suppressed parasitic LDHs ($Zn_5(OH)_8Cl_2\cdot H_2O$, JCPDS No. 72-1444) generation on the Zn anode by hiring GBL (Figure S19 and S20), strongly demonstrating the enhanced Zn reversibility in $ZnCl_2/H_2O$-40GBL electrolyte.

Zn||I_2 battery under high Zn DOD

Conventional AZIBs are usually assembled using the thick Zn anode (15–200 μm), however, the high excess of Zn results in an overstatement of the energy density of AZIBs owing to the low DOD value of Zn anodes. Furthermore, massive metallic Zn used in batteries would likely extend the cycling life of AZIBs, which cannot reflect the Zn reversibility factually. Although the anode-free design can theoretically endow AZIBs with a high energy density, this design significantly sacrifices the cycling life of AZIBs, which limits the actual applications of AZIBs. Taking both energy density and cycling life into account, the future design of AZIBs with a Zn DOD of $\geq 50\%$ will be reliable.

Zn||I_2 battery based on I^-/I_2 conversion presents a high energy density, high out-put potential, and excellent rate capability, which has been recognized as a promising cathode candidature for AZIBs.[20] However, polyiodide shuttling can lead to fast battery degradation by accelerating the active Zn loss.[21] To suppress the polyiodide shuttling, trisodium citrate-derived porous carbon (TCC) was adopted to confine the polyiodide. SEM images reveal that TCC shows a nanoarchitecture with a continuous porous network (Figure S21), which provides adequate space and active sites for iodine storage and polyiodide confinement. I_2 was loaded in TCC by the melt diffusion method with a loading mass of 60 wt%, as demonstrated by thermogravimetric analysis (Figure S22). The Zn||I_2 battery using TCC@I_2 cathode exhibits high specific capacity (215 mAh g^{-1}) and high value of CE (>99.0%) at 0.2 A g^{-1}, validating TCC well confine the polyiodide to suppress the shuttle effect (Figure S23).

Thus, the cycling performance of $Zn||I_2$ full cells under high DOD can well reflect the Zn reversibility. Accordingly, the feasibility of molecular switch on the Zn-based full cell performance was estimated using $Zn||I_2$ batteries with a 50% Zn DOD, which was assembled by matching high-loading I_2@TCC cathode ($\approx 8.0\ mg_{iodine}\ cm^{-2}$, $\approx 1.5\ mAh\ cm^{-2}$), and Cu-supported plated Zn anode (Zn@Cu, $\approx 3.0\ mAh\ cm^{-2}$) $Zn||I_2$ batteries using two electrolytes present a similar specific capacity of $\approx 215\ mAh\ g^{-1}$ under $0.2\ A\ g^{-1}$, corresponding to an area capacity of $\approx 1.6\ mAh\ cm^{-2}$. However, the $Zn||I_2$ battery using $ZnCl_2/H_2O$ electrolyte proceeds a poor rate capability and larger polarization with step-wisely increased current densities compared with the counterpart using $ZnCl_2/H_2O$-40GBL (Figure S24). The cyclability of $Zn||I_2$ batteries under such high Zn DOD was subsequently investigated. As displayed in Figure 5a, $Zn||I_2$ battery using $ZnCl_2/H_2O$ electrolyte shows inferior performance with 77.2% capacity retention after initial 650 cycles at $2\ A\ g^{-1}$ accompanied the significant polarization increases (Figure 5b), implying instable Zn/electrolyte interface. Nevertheless, a sharp capacity fading occurs in the following cycles, which should be attributed to the insufficient zinc supplement, as confirmed by the digital image of Zn@Cu electrode after 1000 cycles with exhausted active Zn (inset in Figure 5a). In sharp comparison, the high Zn reversibility in $ZnCl_2/H_2O$-40GBL could enable high-cyclability $Zn||I_2$ battery with 81.2% capacity retention for 2000 cycles. And only a slight increase in battery polarization manifests the desirable Zn/electrolyte interface (Figure 5b). Argenteous Zn also is observed on the Cu foil after

1000 cycles in $ZnCl_2/H_2O$-40GBL, indicating that the adequate active Zn is preserved (inset in Figure 5a). The corresponding SEM image further reveals that a compact Zn layer well attaches on the Cu substrate after 1000 cycles, emphasizing the superior Zn reversibility in $ZnCl_2/H_2O$-40GBL electrolyte (Figure 5c).

Low-temperature AZIBs

The practical application of AZIBs requires wide-rage operation temperature. Anti-freezing GBL solvent and significant H_2O–GBL interplays significantly extend the freezing point from $-15.5\ °C$ to $-33\ °C$ after hiring 40 vol% GBL in $ZnCl_2/H_2O$ electrolytes (Figure S25). To understand the impact of GBL on reducing the freezing point of electrolytes, Raman spectra were collected to reveal the O–H stretching vibration of water molecules (3000–3700 cm^{-1}) (Figure S26). The O–H stretching vibration can be divided into three components, strong H-bond, weak H-bond, and non H-bond.[22] With the GBL proportion in $ZnCl_2/H_2O$ electrolytes increasing, a significant shift of strong and weak H-bond to high frequency indicates that the H-bond of water is weakened by adding GBL. MD simulation also reveals that the average H-bond number is declined after hiring 40 Vol% GBL compared to the $ZnCl_2/H_2O$ electrolyte (Figure S27). These results demonstrate the function of GBL on breaking strong H-bond network of water, which leads to the freezing point declination of electrolytes. Then, the Zn reversibility under low temper-
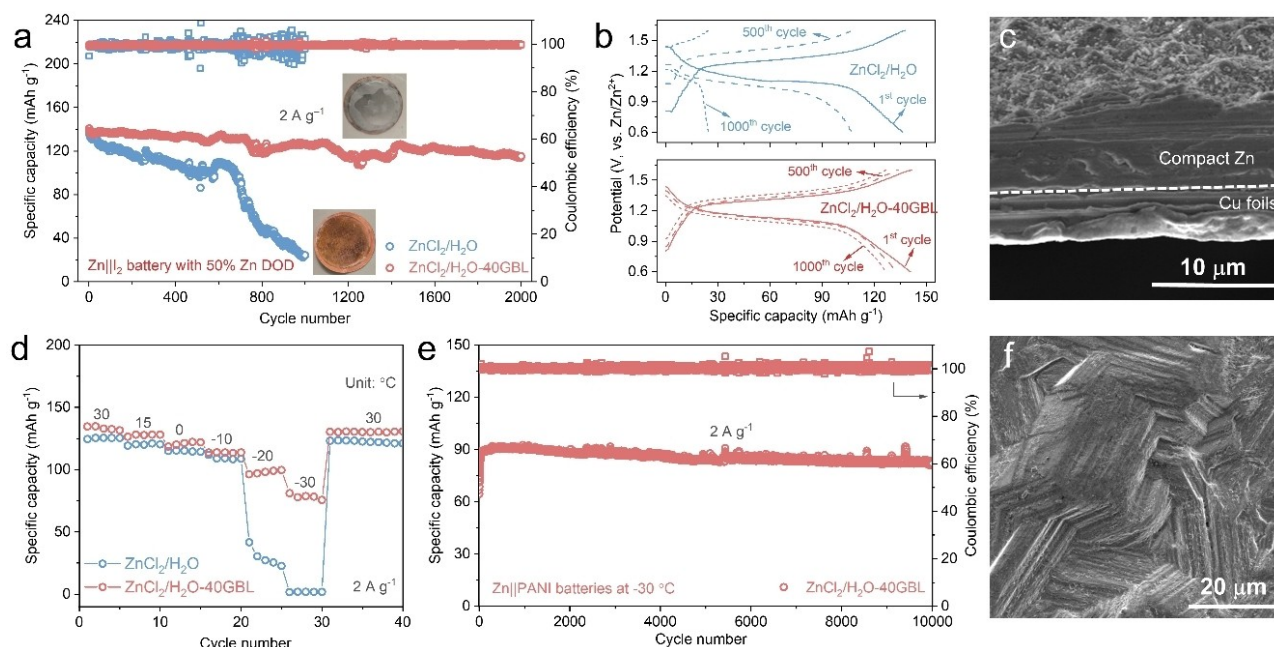

Figure 5. Full-cell configuration. a) Cycling performance and b) Charge-discharge curves of $Zn||I_2$ batteries with a high Zn DOD (50%). Insert in (a) shows the photographs of Cu@Zn anodes after 1000 cycles. c) The cross-section SEM image of Zn@Cu anode in $Zn||I_2$ batteries using $ZnCl_2/H_2O$-40GBL electrolyte after 1000 cycles. d) The specific capacity of $Zn||PANI$ batteries in two electrolytes under different temperatures. e) Cycling performance of $Zn||PANI$ batteries using $ZnCl_2/H_2O$-40GBL electrolyte at $-30\ °C$. f) SEM image of Zn anode after 100 cycles in $Zn||PANI$ batteries at $-30\ °C$.

ature was further investigated. As expected, the ZnCl$_2$/H$_2$O-40GBL electrolyte can also enable high Zn reversibility at low temperatures, as supported by uniform Zn morphology, high average Zn CE (99.5 % at 0 °C and 99.9 % at −30 °C), and steady Zn plating/stripping performance (Figure S28 and S29).

Besides, the PANI electrode was selected as a cathode for the design of low-temperature AZIBs due to its good structural stability. The stepwise declination of temperatures (30 °C to −30 °C) was firstly adopted to investigate the capacity response of Zn‖PANI batteries (Figure 5d). Similar specific capacity delivery in ZnCl$_2$/H$_2$O with/without GBL can be observed under relatively high temperature of ≥ −10 °C. While a violent capacity decay occurs in Zn‖PANI battery using ZnCl$_2$/H$_2$O electrolyte with only 27.2 mAh g^{-1} at −20 °C, much lower than that using ZnCl$_2$/H$_2$O-40GBL electrolyte (99.1 mAh g^{-1}). After further reducing the temperature to −30 °C, the operation of battery using ZnCl$_2$/H$_2$O electrolyte is directly intercepted, this is because the ZnCl$_2$/H$_2$O electrolyte has been frozen under such a low temperature (Figure S30). In contrast, there is a high capacity of 78.8 mAh g^{-1} remaining in Zn‖PANI battery using ZnCl$_2$/H$_2$O-40GBL electrolyte. Corresponding charge–discharge curves further validate the ZnCl$_2$/H$_2$O-40GBL electrolyte can endow superior low-temperature performance with small battery polarization (Figure S31). Subsequently, the long-term cyclability of Zn‖PANI batteries was studied under stringent conditions. The Zn‖PANI battery using ZnCl$_2$/H$_2$O-40GBL electrolyte features a high initial discharge capacity of 125.8 mAh g^{-1} and remains 91.3 % of initial capacity after 2000 cycles at 0 °C, whilst the fast capacity fading is observed in ZnCl$_2$/H$_2$O electrolyte with only 62 % retentive capacity after 650 cycles (Figure S32). The superior anti-freezing ability of ZnCl$_2$/H$_2$O-40GBL electrolyte endows the high cyclability of AZIBs under an extreme temperature of −30 °C. Undoubtably, Zn‖PANI battery in ZnCl$_2$/H$_2$O-40GBL can deliver a high initial capacity of 90.0 mAh g^{-1}, and stable cycling with ignorable capacity fading for 10 000 cycles is realized (Figure 5e). The Zn electrode after 100 cycles still shows the compact and texture-regulating morphology, which further strongly validates the stable and high-reversible Zn anode in GBL-modified electrolyte (Figure 5f). The successful demonstration of AZIBs with distinguished electrochemical superiority under limited Zn supplement and extremely low-temperature conditions strongly verifies the advantage of an as-designed functionalized electrolyte.

Conclusion

In summary, the pH-triggered molecular switch with reversible structure conformations between GBL and GHB is successfully realized to dynamically modulate the Zn/electrolyte interface and enhance the Zn reversibility. During Zn plating, the increased interfacial alkalinity triggers the "on" state of the molecular switch by the GBL-to-GHB transformation. As-generated GHB enables the Zn affinity via triple Zn–O interactions, leading to suppressive

H$_2$ evolution and texture-regulated Zn plating morphology. During Zn stripping, the adsorbed GHB is released to the electrolyte, leading to the "off" state of molecular switch by re-generating GBL through the cyclization reaction. Based on this molecular switch strategy, the Zn reversibility is significantly enhanced with high Zn plating/stripping CE (99.6 % for 500 cycles). Moreover, this GBL-induced interfacial modulation also enables a Zn‖I$_2$ battery with stable a lifespan for 2000 cycles under high Zn DOD of 50 %. This contribution demonstrates a dynamic modulation of Zn/electrolyte interface by molecular switch strategy, which brings new insight into the effective interface design for active metal anodes.

Conflict of Interest

The authors declare no conflict of interest.

Data Availability Statement

The data that support the findings of this study are available from the corresponding author upon reasonable request.

[1] a) D. Chao, W. Zhou, F. Xie, C. Ye, H. Li, M. Jaroniec, S.-Z. Qiao, *Sci. Adv.* **2020**, *6*, eaba4098; b) L. Ma, S. Chen, N. Li, Z. Liu, Z. Tang, J. A. Zapien, S. Chen, J. Fan, C. Zhi, *Adv. Mater.* **2020**, *32*, 1908121; c) J. Hao, L. Yuan, B. Johannessen, Y. Zhu, Y. Jiao, C. Ye, F. Xie, S. Z. Qiao, *Angew. Chem. Int. Ed.* **2021**, *60*, 25114; *Angew. Chem.* **2021**, *133*, 25318.

[2] X. Zhou, H. Jin, B. Y. Xia, K. Davey, Y. Zheng, S. Z. Qiao, *Adv. Mater.* **2021**, *33*, 2104341.

[3] a) Q. Yang, L. Li, T. Hussain, D. Wang, L. Hui, Y. Guo, G. Liang, X. Li, Z. Chen, Z. Huang, Y. Li, Y. Xue, Z. Zuo, J. Qiu, Y. Li, C. Zhi, *Angew. Chem. Int. Ed.* **2022**, *61*, e202112304; *Angew. Chem.* **2022**, *134*, e202112304; b) F. Mo, Z. Chen, G. Liang, D. Wang, Y. Zhao, H. Li, B. Dong, C. Zhi, *Adv. Energy Mater.* **2020**, *10*, 2000035.

[4] a) J. Hao, L. Yuan, C. Ye, D. Chao, K. Davey, Z. Guo, S. Z. Qiao, *Angew. Chem. Int. Ed.* **2021**, *60*, 7366; *Angew. Chem.* **2021**, *133*, 7442; b) L. Cao, D. Li, E. Hu, J. Xu, T. Deng, L. Ma, Y. Wang, X. Q. Yang, C. Wang, *J. Am. Chem. Soc.* **2020**, *142*, 21404; c) F. Ming, Y. Zhu, G. Huang, A. H. Emwas, H. Liang, Y. Cui, H. N. Alshareef, *J. Am. Chem. Soc.* **2022**, *144*, 7160.

[5] a) K. Zhao, G. Fan, J. Liu, F. Liu, J. Li, X. Zhou, Y. Ni, M. Yu, Y. M. Zhang, H. Su, Q. Liu, F. Cheng, *J. Am. Chem. Soc.* **2022**, *144*, 11129; b) A. Bayaguud, X. Luo, Y. Fu, C. Zhu, *ACS Energy Lett.* **2020**, *5*, 3012; c) J. Hao, J. Long, B. Li, X. Li, S. Zhang, F. Yang, X. Zeng, Z. Yang, W. K. Pang, Z. Guo, *Adv. Funct. Mater.* **2019**, *29*, 1903605; d) K. Yang, Y. Hu, T. Zhang, B. Wang, J. Qin, N. Li, Z. Zhao, J. Zhao, D. Chao, *Adv. Energy Mater.* **2022**, *12*, 2202671; e) Z. Wu, M. Li, Y. Tian, H. Chen, S. J. Zhang, C. Sun, C. Li, M. Kiefel, C. Lai, Z. Lin, S. Zhang, *Nano-Micro Lett.* **2022**, *14*, 110.

[6] a) J. Hao, B. Li, X. Li, X. Zeng, S. Zhang, F. Yang, S. Liu, D. Li, C. Wu, Z. Guo, *Adv. Mater.* **2020**, *32*, 2003021; b) M. Liu, J. Cai, H. Ao, Z. Hou, Y. Zhu, Y. Qian, *Adv. Funct. Mater.* **2020**, *30*, 2004885.

[7] a) O. Fitzmaurice, M. Bartkowski, S. Giordani, *Front. Chem.* **2022**, *10*, 859450; b) M. Natali, S. Giordani, *Chem. Soc. Rev.* **2012**, *41*, 4010.

[8] a) M. Takeuchi, M. Ikeda, A. Sugasaki, S. Shinkai, *Acc. Chem. Res.* **2001**, *34*, 865; b) V. V. Samoshin, Y. Zheng, X. Liu, *J. Phys. Org. Chem.* **2017**, *30*, e3689.

[9] a) C. Xu, B. Li, H. Du, F. Kang, *Angew. Chem. Int. Ed.* **2012**, *51*, 933; *Angew. Chem.* **2012**, *124*, 957; b) L. Yuan, J. Hao, C.-C. Kao, C. Wu, H.-K. Liu, S.-X. Dou, S.-Z. Qiao, *Energy Environ. Sci.* **2021**, *14*, 5669.

[10] D. Zhu, Y. Huang, L. Zhang, H. Fan, H. Wang, *J. Electrochem. Soc.* **2020**, *167*, 070513.

[11] S. J. Zhang, J. Hao, D. Luo, P. F. Zhang, B. Zhang, K. Davey, Z. Lin, S. Z. Qiao, *Adv. Energy Mater.* **2021**, *11*, 2102010.

[12] a) R. Gómez-Bombarelli, E. Calle, J. Casado, *J. Org. Chem.* **2013**, *78*, 6868–6879; b) A. J. Sabucedo, K. G. Furton, *J. Sep. Sci.* **2004**, *27*, 703.

[13] J. Li, Y. Zhou, J. Tian, L. Peng, J. Deng, N. Wang, W. Qian, W. Chu, *J. Mater. Chem. A* **2020**, *8*, 10386.

[14] Z. Cao, P. Zhuang, X. Zhang, M. Ye, J. Shen, P. M. Ajayan, *Adv. Energy Mater.* **2020**, *10*, 2001599.

[15] Y. Ikezawa, K. Atobe, *Electrochim. Acta* **2011**, *56*, 7078.

[16] J. S. Chappell, A. W. Meyn, K. K. Ngim, *J. Forensic Sci.* **2004**, *49*, 52.

[17] J. Hao, L. Yuan, Y. Zhu, M. Jaroniec, S. Z. Qiao, *Adv. Mater.* **2022**, *34*, 2206963.

[18] P.-F. Zhang, Z. Wu, S.-J. Zhang, L.-Y. Liu, Y. Tian, Y. Dou, Z. Lin, S. Zhang, *Nano Energy* **2022**, *102*, 107721.

[19] M. Zhou, S. Guo, J. Li, X. Luo, Z. Liu, T. Zhang, X. Cao, M. Long, B. Lu, A. Pan, G. Fang, J. Zhou, S. Liang, *Adv. Mater.* **2021**, *33*, 2100187.

[20] a) L. Ma, Y. Ying, S. Chen, Z. Huang, X. Li, H. Huang, C. Zhi, *Angew. Chem. Int. Ed.* **2021**, *60*, 3791; *Angew. Chem.* **2021**, *133*, 3835; b) W. Li, K. Wang, K. Jiang, *J. Mater. Chem. A* **2020**, *8*, 3785; c) Y. Yang, S. Liang, B. Lu, J. Zhou, *Energy Environ. Sci.* **2022**, *15*, 1192; d) L. Yan, S. Zhang, Q. Kang, X. Meng, Z. Li, T. Liu, T. Ma, Z. Lin, *Energy Storage Mater.* **2023**, *54*, 339.

[21] a) S. J. Zhang, J. Hao, H. Li, P. F. Zhang, Z. W. Yin, Y. Y. Li, B. Zhang, Z. Lin, S. Z. Qiao, *Adv. Mater.* **2022**, *34*, 2201716; b) H. Yang, Y. Qiao, Z. Chang, H. Deng, P. He, H. Zhou, *Adv. Mater.* **2020**, *32*, 2004240; c) Z. Li, X. Wu, X. Yu, S. Zhou, Y. Qiao, H. Zhou, S. G. Sun, *Nano Lett.* **2022**, *22*, 2538; d) K. Wang, J.-B. Le, S.-J. Zhang, W.-F. Ren, J.-M. Yuan, T.-T. Su, B.-Y. Chi, C.-Y. Shao, R.-C. Sun, *J. Mater. Chem. A* **2022**, *10*, 4845.

[22] Q. Zhang, Y. Ma, Y. Lu, L. Li, F. Wan, K. Zhang, J. Chen, *Nat. Commun.* **2020**, *11*, 4463.

Research Articles

Aqeous Zn Batteries

S.-J. Zhang, J. Hao, Y. Zhu, H. Li, Z. Lin,*
S.-Z. Qiao* ─────────────── **e202301570**

pH-Triggered Molecular Switch Toward Tex-
ture-Regulated Zn Anode
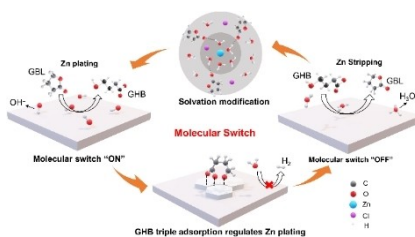
Depending on the periodic pH evolution during Zn plating/stripping, a pH-triggered molecular switch with reversible transformation between γ-butyrolactone and γ-hydroxybutyrate is applied to dynamically modulate the Zn/electrolyte interface. This molecular switch strategy results in texture-regulated Zn plating, suppressive hydrogen evolution, and excellent Zn reversibility even under high depth of discharge.